

Strain monitoring case study: Sutong Cable-stayed Bridge

Hao Wang¹, Jianxiao Mao² and Jian Li³

¹ Key Laboratory of C&PC Structures of Ministry of Education, Southeast Univ., Nanjing, China, wanghao1980@seu.edu.cn

² Key Laboratory of C&PC Structures of Ministry of Education, Southeast Univ., Nanjing, China, jx1990@seu.edu.cn

³ Department of Civil, Environmental, Architectural Engineering, Univ. of Kansas, Lawrence, USA, jianli@ku.edu

ABSTRACT: This case study summarizes the variation features of the strain responses and the fatigue reliability assessments of key welded details of orthotropic steel deck of the longest cable-stayed bridge in China, i.e., Sutong Cable-stayed Bridge, based on the one-year continuous structural health monitoring data. The presented case study is a summary of authors' previous studies; detailed information is available in the previous papers [1-2].

Test Structure and Measured Data

Sutong Cable-stayed Bridge (SCB), with a main span of 1,088 m, is the longest cable-stayed bridge in China. General view of this bridge is shown in Figure 1. It is a critical national artery which connects the cities of Nantong and Suzhou by crossing the Yangtze River and plays an important role in constituting the main framework of the highway network in Jiangsu province of China. Numerous freight and passenger vehicles pass through the bridge daily. In addition, the bridge is located at the mouth of the Yangtze River in the eastern coastal area of China, where meteorological disasters like typhoons happen frequently. Therefore, a comprehensive SHM system has been installed on this bridge for long-term performance assessment.



Figure 1. Sutong Cable-stayed Bridge

Orthotropic steel deck (OSD), a lightweight deck system with high longitudinal stiffness, is employed in the main girder of SCB. Under long-term traffic loads, the welded connections of OSD will be subjected to a combination of localized in-plane and out-of-plane bending stresses, leading to load-induced fatigue cracking. The growth of cracks can potentially result in catastrophic failure of bridge structures. Therefore, the spot-welded electrical resistance strain gauges (RSG) are installed at different sections of the bridge girder to monitor the structural responses induced by traffic and wind loads as an important part of the SHM system. Among different sections distributed along the main girder of SCB, the mid-span section carries the largest bending moment, hence the corresponding strain values are larger than those at other sections. Therefore, to evaluate the fatigue performance of the welded details of the OSD, only the strain gauges installed at the mid-span section are selected in this study.

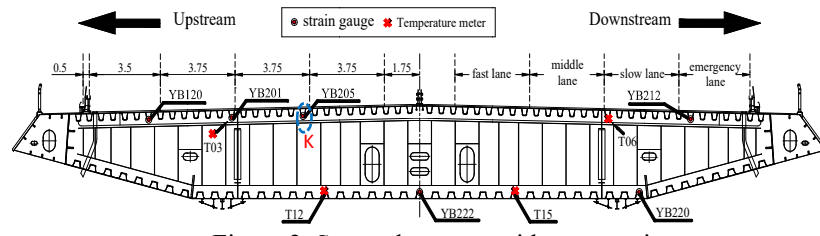


Figure 2. Sensor layout at mid-span section

Orthotropic steel deck (OSD), a lightweight deck system with high longitudinal stiffness, is employed in the main girder of SCB. Under long-term traffic loads, the welded connections of OSD will be subjected to a combination of localized in-plane and out-of-plane bending stresses, leading to load-induced fatigue cracking. The growth of cracks can potentially result in catastrophic failure of bridge structures. Therefore, the spot-welded electrical resistance strain gauges (RSG) are installed at different sections of the bridge girder to monitor the structural responses induced by traffic and wind loads as an important part of the SHM system. Among different sections distributed along the main girder of SCB, the mid-span section carries the largest bending moment, hence the corresponding strain values are larger than those at other sections. Therefore, to evaluate the fatigue performance of the welded details of the OSD, only the strain gauges installed at the mid-span section are selected in this study.

Among all fifty-six strain gauges installed at the mid-span section of SCB, six strain gauges (YB120, YB201, YB205, YB212, YB220, and YB222) located at the U ribs along the longitudinal direction are selected to analyze the global mechanical responses of OSD, including the slow-varying trend and vehicle induced stress cycles. The layout of the strain sensors at the mid-span section of SCB are shown in Figure

2. The strain gauge is 60 mm long and is protected by the stainless-steel cover. The sampling frequency of the strain gauges is 10 Hz. Four strain gauges (YB120, YB201, YB205, and YB212) are installed at the top flange of OSD, while the other two (YB220, and YB222) installed at the bottom flange. In addition, four temperature sensors (T03, T06, T12, and T15) are used to assess the correlation between strain varying trend and temperature change. Furthermore, four strain gauges around the U rib K, as shown in Figure 3, are utilized to conduct fatigue reliability assessment of the welded details. The sensors YB203, YB205, and YB206 are strain gauges measuring longitudinal strain responses, while YB204 measures the transverse ones.

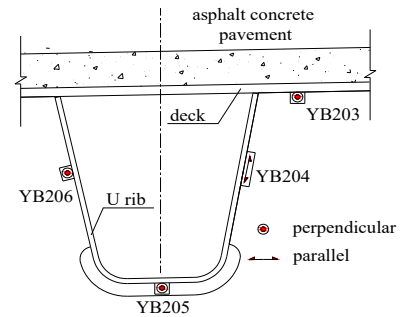


Figure 3. Strain gauges around U rib K

The measured 24-hour strain responses of YB205 on Jan. 7, 2009 are shown in Figure 4(a). The strain responses are composed of two components, namely, the slow-varying component and the dynamic component. The slow-varying trends are extracted using MAM and results show that it has the similar variation trend with the structural temperature. After the slow-varying trends of the strain responses are removed using MAM, the remaining components, namely as the dynamic strain responses, can be used to represent the dynamic loading effects of traffic and wind. The dynamic strain responses of YB205 on August 10th are displayed in Figure 4(b), which contain higher-frequency signals with the maximum amplitude close to $350\mu\epsilon$.

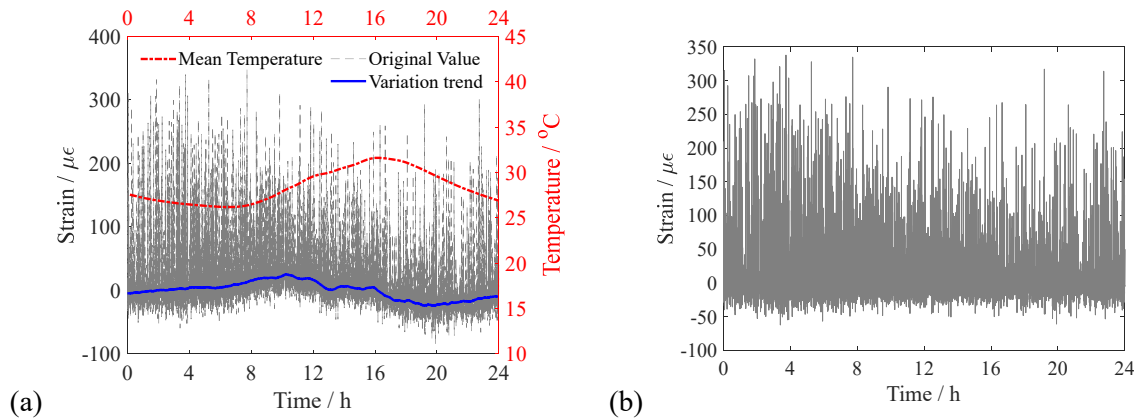


Figure 4. Recorded 24-h strain responses of YB205. (a) Original signal; (b) Dynamic component.

SHM Methodology and Results

The slow-varying trend of strain responses is firstly eliminated with the combination of moving average method and padding scheme, and the dynamic strain responses are obtained. After that, the dynamic strain responses are transformed into stress values according to the Hooke's law with the modulus of 210,000 MPa. The stress-range histograms of the selected strain gauges, i.e., YB120, YB201, YB205, YB212, YB220, and YB222, are obtained using the rainflow cycle counting algorithm which includes four steps, i.e., hysteresis filtering, peak-valley filtering, discretization, and four-point cycle counting. On that basis, the lognormal probability distribution function (PDF) is applied to fit the distribution of the estimated stress

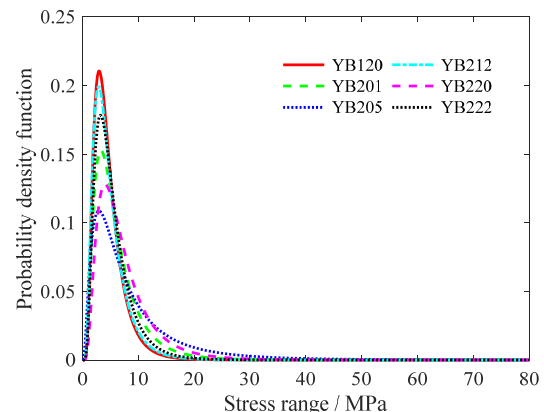


Figure 5. Fitted stress range PDFs

ranges PDFs are shown in Figure 5. Afterwards, the equivalent stress ranges S_{re} of the selected strain gauges are calculated according to the equations listed in [1]. Based on the continuously monitored strain responses by the SHM system, the daily equivalent stress ranges and stress cycles during 2009 were calculated and shown in Figure 6.

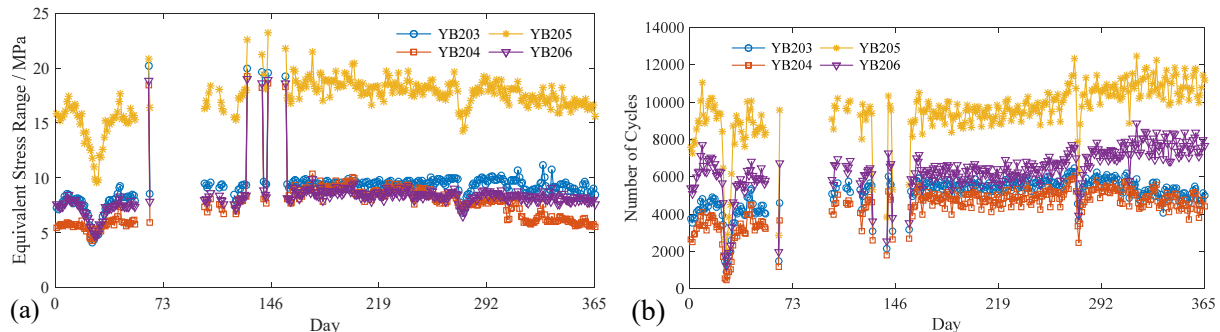


Figure 6. Calculated daily: (a) equivalent stress range; and (b) number of cycles in 2009

The lifetime fatigue reliability of three welded details of orthotropic steel deck will be investigated, including rib-to-deck at diaphragm (RTDD), rib-to-diaphragm (RTD), and diaphragm-to-deck (DTD) details. The fatigue crack of RTDD would be evaluated with YB204. The fatigue crack of RTD will be evaluated with YB205 and YB206. The fatigue crack of DTD will be evaluated with YB203. Following the limited state function of Miner's damage accumulation index, the fatigue reliability of three welded details are estimated using the field-monitoring stress ranges and cycles. The estimated time-dependent fatigue reliability indexes are shown in Figure 7.

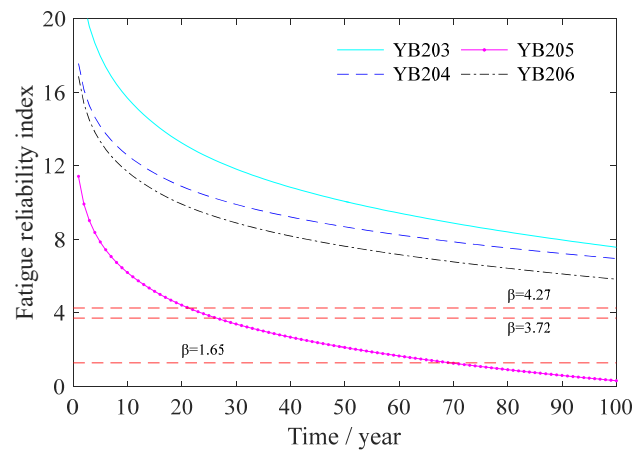


Figure 7. Fatigue reliability indexes of welded details

Lessons Learned

This case study demonstrated the feasibility of performing detailed evaluation of fatigue reliability of the welded details with field-monitored strain responses. The presented results can provide valuable references for the fatigue-resistance design, construction, operation, and maintenance of long-span bridges and add to our knowledge about the operational conditions of these bridges in terms of serviceability, strength, and reliability.

Acknowledgements

The authors would like to gratefully acknowledge the support from the National Natural Science Foundation of China (Grant No. 51722804). The support from the Jiangsu Health Monitoring Data Center for Long-span Bridges is also acknowledged.

References

- [1] Jianxiao Mao, Hao Wang, Jian Li. Fatigue reliability assessment of a long-span cable-stayed bridge based on one-year monitoring strain data, *Journal of Bridge Engineering*, 2018: 24(1), 05018015.
- [2] Hao Wang, Tianyou Tao, Aiqun Li, Yufeng Zhang. Structural health monitoring system for Sutong cable-stayed bridge, *Smart Structures and Systems*, 2016, 18(2): 317-334.